CrossMark

ORIGINAL

D. Čakmak · H. Wolf · Ž. Božić · M. Jokić

Optimization of an inerter-based vibration isolation system and helical spring fatigue life assessment

Abstract This paper presents an analytical analysis and optimization of vibration-induced fatigue in a generalized, linear two-degree-of-freedom inerter-based vibration isolation system. The system consists of a source body and a receiving body, coupled through an isolator. The isolator consists of a spring, a damper, and an inerter. A broadband frequency force excitation of the source body is assumed throughout the investigation. Optimized system, in which the kinetic energy of the receiving body is minimized, is compared with suboptimal systems by contrasting the fatigue life of a receiving body helical spring with several alternative isolator setup cases. The optimization is based on minimizing specific kinetic energy, but it also increases the number of cycles to fatigue failure of the considered helical spring. A significant portion of this improvement is due to the inclusion of an optimally tuned inerter in the isolator. Various helical spring deflection and stress correction factors from referent literature are discussed. Most convenient spring stress and deflection correction factors are adopted and employed in conjunction with pure shear governed proportional stress in the context of high-cycle fatigue.

1 Introduction

Mechanical systems, e.g. car suspension systems [1,2] are often subjected to high dynamic loading during their lifetime. Such service loadings can cause unwanted vibration and premature failure, resulting from destructive fatigue mechanisms [3]. These are especially evident in case of resonant harmonic excitations [1,3]. Heavy-duty springs used in car suspension systems [1,2] are an example where a crack may initiate at a stress concentration location and further propagate, potentially leading to a catastrophic failure [3–5]. Considering vibration fatigue modelling and analysis of helical springs, both stiffness and strength parameters of general vibration system should be determined for adequate mathematical modelling, which can be found in [6–18]. Classical works on strength of materials [19,20], elasticity theory [21] and recent mechanical engineering literature [22,23] touch on the subject of spring durability and spring fatigue. Considering springs as machine elements that need to withstand exceptionally long life, appropriate high-cycle fatigue (HCF) calculation method [23–28] is usually utilized for fatigue lifetime assessment. Extensive studies on the spring fatigue life, particularly for helical springs, have been conducted [28–34].

From related literature [6–11], it can be observed that various stress and deflection correction factors are used for spring strength analysis by different authors. Most often applied stress correction factors are those introduced by Wahl [6,7,10,11,14–17,19–23], Bergsträsser [10,11,14,17,22] and Göhner [7–9,14,17]. For

D. Čakmak (✉) · H. Wolf · Ž. Božić · M. Jokić
University of Zagreb, Faculty of Mechanical Engineering and Naval Architecture, I. Lučića 5, 10000 Zagreb, Croatia
E-mail: damjan.cakmak@fsb.hr
Tel.: +385 1 6168 426

example, German DIN standard on calculation and design of cylindrical helical springs was previously based on Göhner [8,9]; however, it is now based on the Bergsträsser and Wahl [10,11] correction factors. The stress correction factors may significantly influence predicted fatigue lifetime of helical springs. Wahl himself in his work [7] suggests that application of his own stress correction factor may result in over-conservative fatigue life prediction. However, e.g. SAE [15] and Ugural [23] recommend using Wahl's stress correction factor, especially for fatigue analysis. Shigley [22], for instance, recommends the Bergsträsser's correction factor for fatigue lifetime assessment, for engineering simplicity reasons; however, he does not advise against using Wahl.

Regarding helical spring fatigue, Berger and Kaiser [28,29] analysed results of very high-cycle fatigue (VHCF) tests on helical compression springs up to 10^9 cycles, where they observed that cracks tend to occur below the surface beyond 10^7 cycles, which is a practical upper limit for HCF. The authors also mentioned that Göhner and Bergsträsser correction factors could yield too conservative results in a fatigue life assessment, which is in agreement with Wahl [7]. Commonly, fatigue life assessment of mechanical springs is based on fatigue endurance to torsion shear [19–23]. Contrary to that, Del Llano-Vizcaya et al. [30] point out that during fatigue testing of compression springs with large index (coil radius to wire radius ratio), the dominant fatigue cracks are initiated and propagated by variation of the principal tensile stress, rather than by the maximum shear stress. Pyttel et al. [31] used Wahl stress correction factor and finite element method (FEM) for helical spring stress analysis. Rivera et al. [32] also used Wahl stress correction for spring for elevator doors analytical fatigue analysis. On the other hand, Ružička et al. [33] used Göhner [8,9,14] and Ancker & Goodier [12,14] stress correction factor for analytical spring fatigue study and compared it with FEM results. Kamal et al. [34] used FEM for both stress ($S - N$) and strain-life fatigue ($\varepsilon - N$) analysis of helical spring.

Contemporary literature dealing with vibration and dynamic problems tied to fatigue, e.g. [1,3–5] do not yet incorporate the beneficiary usage of inerter [2,35] in a classical mass-damper-spring (MDS) environment. In mechanical networks, inerter is a relatively novel element developed by Smith [2] which produces force proportional to relative acceleration ($a_2 - a_1$) between its terminals, i.e. relation $F_{inrt} = b(a_2 - a_1)$ holds. The coefficient of inerter resistance force F_{inrt} is called *inertance*. It is denoted by label "b" and is measured in kilograms. Ideal inerter can be approximated in the same sense in which mathematical ideals approximate, e.g. springs and viscous dampers. Ideally, it is assumed that its mass is small compared to produced inertance [2]. According to authors' knowledge, no attempt to include the ideal inerter concept in commercial FEM codes is recorded in the literature.

In the presented study, analytical investigation is conducted to model the fatigue load of a helical spring acting as an elastic element in a simple and physically transparent two-degree-of-freedom (2-DOF) inerter-based vibration isolation system. In Sect. 2, analytical mathematical 2-DOF inerter-based vibration isolation system model is established where optimized parameters for both viscous damper and inerter are determined. Minimization of kinetic energy is used as a criterion. In Sect. 3, different dimensionless spring deflection and stress correction factors available from referent literature are discussed, which are later used in the context of analytically determining displacement and stress amplitudes under harmonic force loading. Finally, Sect. 4 presents a benchmark example by utilizing previously adopted optimization model and employing adopted spring correction factors. Benchmark is performed by comparing vibration fatigue study of systems with optimized parameters to sub-par systems. Method for deriving the optimal damping and optimal inertance combined with optimal damping is developed and employed. Göhner-, Castigliano- and Timoshenko-based deflection correction factor is derived in dimensionless form. There is no record in the literature of employing Timoshenko thick beam formulation [19–21] and Cowper shear correction factor [36] for spring deflection correction, which is also investigated in the scope of this paper, where novel deflection correction factor is derived. Analytical expression based on the von Mises criterion [22,27,37] for shear governed biaxial and proportional stress, which explicitly ties vibration displacement amplitudes through Basquin's equation with HCF of helical spring, is derived and given in explicit form.

2 2-DOF inerter-based vibration isolator mathematical model

In this chapter, the generalized analytical mathematical model for discrete 2-DOF inerter-based vibration isolation system is established analytically. The studied problem is represented by a discrete parameter model as shown in Fig. 1a. It is assumed that the critical component concerning fatigue is a helical spring k_3, also shown in Fig. 1b where E is (Young) modulus of elasticity, v is Poisson's factor/ratio, S'_f is fatigue strength coefficient, and "B" is Basquin's exponent, i.e. fatigue strength exponent [24,25] here denoted in capital letter in order not to be confused with inertance "b". Number of active coils is denoted as n ($n = 2$ in Fig. 1b),
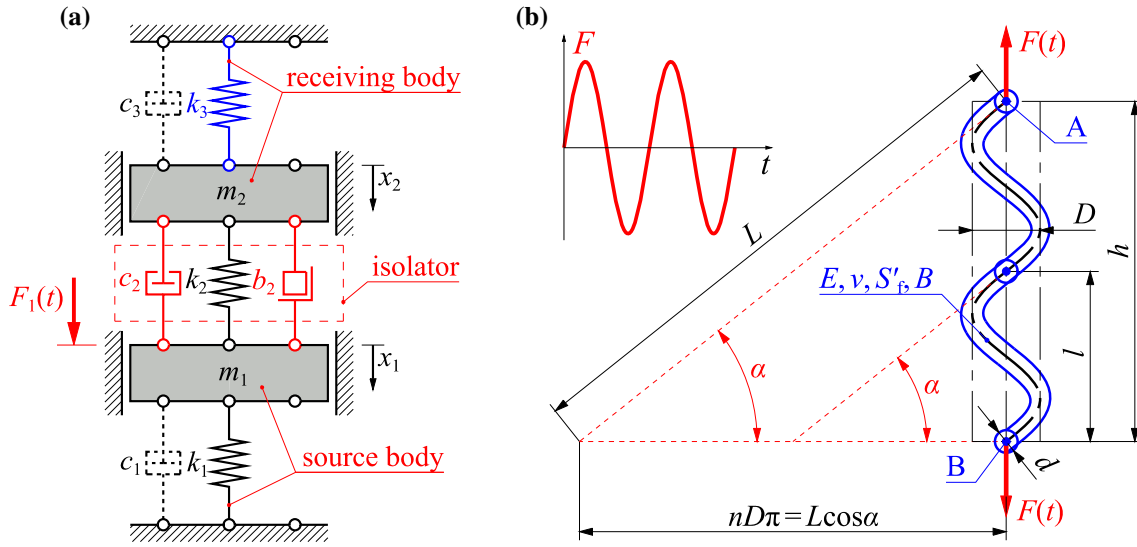
Fig. 1 a The 2-DOF linear discrete vibration isolation system, **b** helical spring k_3 properties (colour figure online)

and h is spring length where $h = n \cdot l$. Diameters D and d are large and small spring diameters, respectively, and $C = D/d$ is defined as spring index [7,22,23]. D can also be designated as the mean coil diameter and d as the wire diameter [22]. Recommended values of spring index C for practical purposes lie between $C = 4 - 12$ [22]. Angle α represents the pitch angle which can be calculated according to geometric expression $\alpha = \arctan[l/(\pi D)]$, where l is the spring pitch. For the time being, the spring stress is not considered and spring stiffness is denoted simply as "k_3".

The goal of the vibration-based optimization is to minimize vibrations of the *receiving body*, i.e. vibrations of mass m_2 which are *proportional* to the maximum deflection amplitudes of spring k_3. In this optimization, the excitation of the *source body* $F_1(t)$ is assumed to have white noise spectral properties [38], i.e. unit loading amplitude $F_{01}(\Omega) = 1$ over all frequencies. The whole vibration system consists of discrete masses m_1 and m_2, ideally massless springs k_1, k_2 and k_3, viscous dampers c_1, c_2 and c_3 and an ideal inerter of inertance b_2. Isolator consists of spring k_2, damper c_2 and inerter b_2. The ideal inerter produces a force F_{inrt} proportional to the relative acceleration [2] between masses m_1 and m_2. Presented discrete parameter approximation may represent a system of a much more complex nature, including structures with distributed mass, stiffness and damping, as discussed in, for example, [39–41].

The equations of motion [1] for system in Fig. 1a can be written in the general matrix form as

$$\mathbf{M}\ddot{\mathbf{x}}(t) + \mathbf{C}\dot{\mathbf{x}}(t) + \mathbf{K}\mathbf{x}(t) = \mathbf{F}(t), \tag{1}$$

where $\mathbf{M}$ is the global mass matrix, $\mathbf{C}$ is the global damping matrix, $\mathbf{K}$ is the global stiffness matrix and $\mathbf{F}(t)$ is the excitation column force vector. Displacement of the masses m_1 and m_2 from their static equilibrium positions, velocity and acceleration vectors are denoted by $\mathbf{x}(t)$, $\dot{\mathbf{x}}(t)$ and $\ddot{\mathbf{x}}(t)$, respectively.

Global matrices and vectors from Eq. (1) can be written as

$$\mathbf{M} = \begin{bmatrix} m_1 + b_2 & -b_2 \\ -b_2 & m_2 + b_2 \end{bmatrix}, \quad \mathbf{C} = \begin{bmatrix} c_1 + c_2 & -c_2 \\ -c_2 & c_2 + c_3 \end{bmatrix}, \quad \mathbf{K} = \begin{bmatrix} k_1 + k_2 & -k_2 \\ -k_2 & k_2 + k_3 \end{bmatrix}, \tag{2a, b, c}$$

$$\mathbf{x} = \begin{bmatrix} x_1(t) \\ x_2(t) \end{bmatrix}, \quad \mathbf{F} = \begin{bmatrix} F_1(t) \\ 0 \end{bmatrix}, \tag{3a, b}$$

where the parameters and functions in the matrices and vectors are denoted in Fig. 1a.

As the damping of the source and receiving bodies is assumed to be fairly light, the effects of the source mass m_1 and the receiving mass m_2 dampers are further neglected, i.e. $c_1 \approx c_3 \approx 0$.

By assuming harmonic excitation and expressing the excitation and the steady-state response in the complex form $\mathbf{F}(t) = \mathbf{F}_0 e^{i\Omega t}$ and $\mathbf{x}(t) = \mathbf{x}_0 e^{i\Omega t}$, where $i = \sqrt{-1}$, the solution of Eq. (1) can be written as

$$\mathbf{x}_0(\Omega) = \left[-\Omega^2 \mathbf{M} + i\Omega \mathbf{C} + \mathbf{K} \right]^{-1} \mathbf{F}, \tag{4}$$

where terms inside the square bracket denote dynamic stiffness matrix and $\mathbf{x}_0(\Omega)$ is the complex displacement amplitude. Differentiating Eq. (4) with respect to time t yields with complex velocity amplitude expression

$$\dot{\mathbf{x}}_0(\Omega) = i\Omega \mathbf{x}_0(\Omega).$$ (5)

By considering $\mathbf{M}$, $\mathbf{C}$ and $\mathbf{K}$ matrices from Eq. (2a, b, c), the steady state, i.e. time-invariant complex response of mass m_2 can be expressed in simplified form as the following frequency response function (FRF)

$$\dot{x}_{02}(\Omega) = \frac{B_0 + (i\Omega) B_1 + (i\Omega)^2 B_2 + (i\Omega)^3 B_3}{A_0 + (i\Omega) A_1 + (i\Omega)^2 A_2 + (i\Omega)^3 A_3 + (i\Omega)^4 A_4}.$$ (6)

where coefficients $A_0 - A_4$ and $B_0 - B_3$ with respect to Eq. (6) are given by

$$\begin{array}{ll} A_0 = (k_2 + k_3) k_1 + k_2 k_3 & B_0 = 0 \\ A_1 = c_2 (k_1 + k_3) & B_1 = k_2 \\ A_2 = (m_2 + b_2) k_1 + (m_1 + m_2) k_2 + (m_1 + b_2) k_3 & B_2 = c_2 \\ A_3 = c_2 (m_1 + m_2) & B_3 = b_2 \\ A_4 = (m_2 + b_2) m_1 + b_2 m_2 \end{array}$$ (7a–i)

The transfer mobility, i.e. FRF $\dot{x}_{02} \equiv v_{02}$, from Eq. (6) represents the complex velocity amplitude of the receiving body per unit forcing $F_{01} = 1$, of the source body. FRF from Eq. (6) is further used to assess the effectiveness of the vibration isolation.

Considering that the excitation force F_1 with unit power spectral density (PSD) is assumed, the specific kinetic energy of the receiving body I_k (per unit mass and per unit excitation force) can be calculated as

$$I_k = \int_{-\infty}^{\infty} \left| \frac{v_{02}(\Omega)}{F_{01}} \right|^2 d\Omega,$$ (8)

according to [42]. The specific kinetic energy index I_k from Eq. (8) is used throughout this study as a quantitative measure of the broadband frequency vibration isolation performance. The objective is to minimize this quantity for all vibration isolation systems analysed in the scope of this paper. Vibration-based isolation optimization with the goal of vibration reduction by using the minimization of kinetic energy can be found in [38]. The specific kinetic energy index in Eq. (8) for I_k can according to [42] analytically be calculated with expression

$$I_k = \pi \frac{A_0 B_3^2 (A_0 A_3 - A_1 A_2) + A_0 A_1 A_4 \left(2 B_1 B_3 - B_2^2\right) - A_0 A_3 A_4 \left(B_1^2 - 2 B_0 B_2\right) + A_4 B_0^2 (A_1 A_4 - A_2 A_3)}{A_0 A_4 \left(A_0 A_3^2 + A_1^2 A_4 - A_1 A_2 A_3\right)},$$ (9)

where substituting coefficients $A_0 - A_4$ and $B_0 - B_3$ from Eq. (7a–i) into Eq. (9) yields with final kinetic energy index I_k analytical expression, which is here omitted because of length.

In the next two subchapters of this study, two types of vibration transmission control are analysed with respect to potential opportunity of minimizing the specific kinetic energy index I_k: isolation control without inerter, i.e. $b_2 = 0$, and isolation control with optimized inertance b_{opt}. Optimized damping and inertance isolator parameters, for inerter excluded where $c_2 = c_{opt}$, and inerter included where $c_2 = c_{opt2}$ and $b_2 = b_{opt}$, are obtained by minimizing the frequency averaged kinetic energy of the receiving body denoted symbolically in Eq. (9).

2.1 Isolation optimization without inerter

By setting the inertance $b_2 = 0$, and considering Eq. (7a–i), Eq. (9) now morphs into simpler form

$$I_k(b_2 = 0) = \pi \frac{k_2^2 (m_1 + m_2) + c_2^2 (k_1 + k_3)}{c_2 (m_2 k_1 - m_1 k_3)^2}.$$ (10)

Differentiating Eq. (10) with respect to viscous damping coefficient c_2, equalling with zero and again solving for damping c_2 yields the single physically valid solution

$$c_{opt} = k_2 \sqrt{\frac{m_1 + m_2}{k_1 + k_3}},$$ (11)

which unambiguously represents the optimum damping coefficient $c_2 = c_{opt}$. Inserting Eq. (11) into Eq. (10) yields the value of optimum, i.e. minimum kinetic energy

$$I_{kopt} = 2\pi k_2 \frac{\sqrt{(m_1 + m_2)(k_1 + k_3)}}{(m_2 k_1 - m_1 k_3)^2}. \tag{12}$$

By inspecting Eq. (12) mathematical structure, two main conclusions can be drawn.

Firstly, optimum kinetic energy I_{kopt} is directly proportional to value of isolator spring stiffness k_2, which strongly implies using soft/compliant spring for better isolation effect. Trivial solution is to incorporate zero stiffness spring k_2 which completely decouples the source and receiving bodies. In practical situations, static or stationary deflections impose true physical limits to spring compliance, therefore spring stiffness k_2 cannot be optimized arbitrarily and is further considered as fixed value.

Secondly, when values $m_2 k_1 \approx m_1 k_3$, denominator of Eq. (12) tends to zero and I_{kopt} value tends to infinity; therefore, such vibration system should be accordingly detuned during design, i.e. $m_2 k_1 \neq m_1 k_3$.

2.2 Isolation optimization with inerter

When $b_2 \neq 0$, differentiating Eq. (9) with respect to damping c_2, equalling with zero and again solving for damping c_2 yields the single physically valid solution

$$c_2 (b_2 \neq 0) = \sqrt{\frac{m_1 + m_2}{k_1 + k_3} k_2^2 - 2b_2 k_2 + \frac{m_1 k_3^2 + m_2 k_1^2 + b_2 (k_1 + k_3)^2}{(k_1 + k_3)[m_1 (b_2 + m_2) + b_2 m_2]} b_2^2}, \tag{13}$$

where c_2 now represents optimum damping $c_{opt}(b_2)$ for any given inertance b_2. For inertance $b_2 = 0$, Eq. (13) morphs into simple Eq. (11). By substituting Eq. (13) into Eq. (9), differentiating with respect to b_2, equalling with zero and solving for b_2, optimum inertance parameter b_{opt} is obtained. Inserting $b_2 = b_{opt}$ into Eq. (13) results with optimum damping c_{opt2}, which subsequently yields an expression for a minimum specific kinetic energy I_{kopt2} from Eq. (9). Analytical expressions for b_{opt}, c_{opt2} and I_{kopt2} are not explicitly shown in the scope of this paper because they are rather cumbersome and very lengthy. However, it is important to note that no numerical approximation is used in the process of optimization, thus all derived expressions are purely algebraic and exact, without any loss in accuracy.

3 Helical spring displacement and stress correction factors

In this chapter, spring stiffness and stress are discussed. A simple expression for determining the spring fatigue life is also derived, where HCF life [22–26] above 10^3 cycles is addressed and employed. Obtained displacement amplitudes in the frequency domain from previous chapter, i.e. Eq. (4), can now be tied to stress amplitudes below the yielding strength σ_Y, necessary for performing vibration fatigue analysis.

Cylindrical spring can for simplicity be viewed as a thin/slender, curved rod/beam subjected to torsion load exclusively. In such case [22], analytical expressions for spring stiffness, static displacement and shear stress can be denoted with

$$k_{nom} = \frac{F_0}{\delta_{nom}} = \frac{Gd^4}{8D^3 n} = \frac{Gd}{8C^3 n} \quad \Rightarrow \quad \delta_{nom} = \frac{8F_0 D^3 n}{Gd^4} = \frac{8F_0 C^3 n}{Gd}, \quad \tau_{nom} = \frac{8F_0 D}{\pi d^3} = \frac{8F_0 C}{\pi d^2}, \tag{14a, b, c}$$

where k_{nom} is nominal spring stiffness, δ_{nom} is nominal spring deflection, τ_{nom} is nominal spring shear stress and $G = E/[2(1 + \nu)]$ is the shear modulus. As linear elastic/small deformation and deflection conditions are assumed, Eq. (14a, b, c) is valid for both tensile and compressive applied force amplitude $\pm F_0$. For simple harmonic loading conditions adopted, $F(t) = F_0 e^{i\Omega t}$. Helical spring geometry, parameters, loading and boundary conditions (BCs) are the same as schematically shown in Fig. 1b. For a more general approach in the scope of this paper, boundaries of spring index C are varied both inside and outside of recommended values $C = 4 - 12$, in order to parametrically test all physically obtainable solutions. As already noted, Eq. (14a, b, c) is obtained by simply considering spring as a thin beam/rod loaded with exclusively torsion shear, where direct shear, curvature and pitch angle effects are ignored and neglected for simplicity. Therefore,
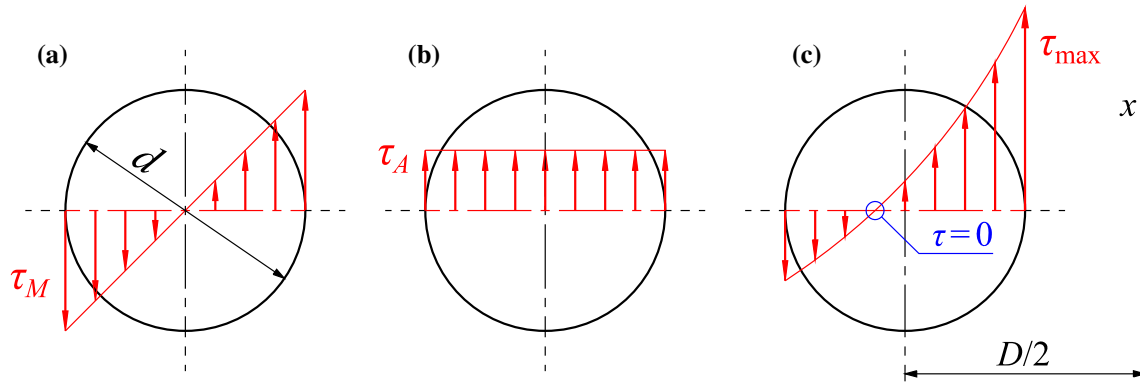
Fig. 2 Spring shear stresses: **a** torsion shear τ_M, **b** transverse/direct shear τ_A, **c** combined torsion and direct shear with additional curvature "c" and pitch angle α effects $\tau_{max} = \tau_M + \tau_A + \tau_c + \tau_\alpha$ (colour figure online)

Table 1 Expressions for stress correction factors K_τ and deflection correction factors K_δ

Author/standard	Stress correction factor K_τ	Deflection correction factor K_δ
Strength of materials		
Wahl, DIN 13906	$\frac{4C-1}{4C-4} + \frac{k_W}{C} = \frac{4C-1}{4C-4} + \frac{1+2\nu}{2(1+\nu)C}$	–
Röver	$\cos(\alpha)\left[\frac{C}{C-\cos^2(\alpha)} + \frac{1+\sin^2(\alpha)}{4C}\right]$	–
Wood	$\frac{C}{C-1} + \frac{1}{2C}$	$\frac{2C^2+C-1}{2C^2}$
Honegger	$\cos(\alpha)\left[\frac{C}{C-\cos^2(\alpha)} + \frac{0.615}{C}\right]$	$\frac{2C^2-\cos^4(\alpha)}{2C^2\cos^5(\alpha)}$
Elasticity theory		
Göhner, DIN 2089	$1 + \frac{5}{4C} + \frac{7}{8C^2} + \frac{1}{C^3}$	$\cos(\alpha) + \frac{3\cos^5(\alpha)}{16(C^2-1)} + \frac{\sin(\alpha)\tan(\alpha)}{1+\nu}$
Ancker & Goodier	$1 + \frac{5}{4C} + \frac{7}{8C^2} + \frac{1}{2}\tan^2(\alpha)$	$1 - \frac{3}{16C^2} + \frac{3+\nu}{2(1+\nu)}\tan^2(\alpha)$
Approximate/empirical relation		
Bergsträsser, DIN 13906	$\frac{C+0.5+\sin^2(\alpha)}{C-0.75+1.51\sin^2(\alpha)}$	–
Sopwith, BS 1726	$\frac{C+0.2}{C-1}$	–
Strain energy (Castigliano's) method		
Shigley	–	$1 + \frac{1}{2C^2}$
Dym	–	$\left(1 + \frac{1}{2C^2}\right)\cos(\alpha) + \left(1 + \frac{1}{4C^2}\right)\frac{\tan(\alpha)\sin(\alpha)}{(1+\nu)}$

additional correction factors K_δ and K_τ need to be applied for displacement and shear stress, where relations $\delta_{max} = K_\delta \delta_{nom}$ and $\tau_{max} = K_\tau \tau_{nom}$ now hold [22,23]. Figure 2 schematically shows spring cumulative shear stress τ correction.

Shift of the helical spring neutral line towards outside of wire diameter d centre results with maximum shear stress τ_{max} appearing at the point closest to spring axis x, as shown in Fig. 2c. As already pointed out in introduction, multiple expressions for correcting deflection and stress exist in the referent literature where authors sometimes present notably different correction factors depending on the theory they used for derivation [15]. Therefore, no unified solution can be found in the literature [14] or standards [8–11].

Table 1 sums up all the expressions from the referent literature used in the scope of this paper.

It is appropriate to recognize that important and thorough investigation regarding spring stress and deflection correction determination was conducted by the *Research Committee on the Analysis of Helical Spring* [14]

where authors parametrically compared influence of spring parameters on stress results based on the theory used. They used FEM for numerical part of the investigation. They obtained the best correlation for Bergsträsser and Göhner stress correction factors and found Wahl to be overly conservative; however, they neglected the influence of pitch angle α on stress correction where $\alpha = 0$ in their main FEM test model for stresses (see Table 5 and Fig. 20 in [14]).

Some data in Table 1 (most notably Wahl, Röver, Wood, Honegger, Göhner, Ancker & Goodier, Bergsträsser and Sopwith) are adopted from already mentioned *Research Committee* [14]. Wahl stress correction factor can also be found in current DIN 13906 (germ. *Deutsches Institut für Normung*) standard [10,11], and [6,7] among others. DIN 13906 [10,11], and [22] also include Bergsträsser stress correction factor, however without pitch angle α inclusion. Göhner stress correction factor, previously included in older, now defunct DIN 2089 [8,9] was later adopted by Ancker & Goodier [12] and rearranged in order to contain initial pitch angle α. By comparing it to original Göhner stress correction expression, it can be observed that the first three terms are identical; however, Göhner uses $1/C^3$, and Ancker & Goodier use $1/2 \cdot \tan^2(\alpha)$ as a last term instead, which takes into account the initial pitch angle α. Ancker & Goodier deflection correction factor from Table 1 can also be found in their original paper [12] and is considered to be one of the most accurate ones found in the literature [16]. Sopwith stress correction factor was used as a part of BS 1726 (British Standard) [16]. Both Shigley [22] and Dym [13] give similar solutions for deflection correction, based on strain energy (Castigliano) method, where Shigley solution is simpler; however, it neglects the influence of pitch angle α compared to Dym.

An additional comment is presented for Wahl stress correction factor, as shown in the first row of Table 1. Nominal expression for Wahl stress factor found in most literature, e.g. [6,7,16] is

$$K_{\tau,\text{Wahl}} = \frac{4C - 1}{4C - 4} + \frac{0.615}{C}. \tag{15}$$

Wahl in his textbook [7] cited Timoshenko [21] as an influence and main source for determining his often cited stress correction factor. It is interesting to observe the numerator of second term from Eq. (15), which is for the sake of this discussion temporarily denoted as $k_W = 0.615$. Wahl used Timoshenko solution which comes from setting a Poisson's ratio $\nu = 0.3$ in the equation derived for the shear stress at the horizontal edge of a cantilevered circular bar [21]. Using the dimensionless, Poisson's ratio ν dependent term found in Eq. (h), p. 321 from [21], one can write expression

$$K_{\tau,\text{Wahl}} = \frac{4C - 1}{4C - 4} + \frac{k_W}{C} \quad \Rightarrow \quad k_W = \frac{1 + 2\nu}{2(1 + \nu)}, \tag{16a,b}$$

and by setting the different values for Poisson's factor ν in Eq. (16b), values of k_W are obtained as

$$k_W(\nu = 0) = 0.5, \quad k_W(\nu = 0.3) = \frac{8}{13} \cong 0.615384615 \approx 0.615, \quad k_W(\nu = 0.5) = 0.\dot{6}, \tag{17a,b,c}$$

where it can be observed that if ν rises, k_W also rises, resulting in larger stress correction factor $K_{\tau,\text{Wahl}}$. By using fixed $k_W = 0.615$, one hard-codes universal, Poisson's ratio-independent stress correction solution. As stresses in helical spring are mostly shear governed [22,23], by adopting the von Mises energy criterion [19–22] with relation $\sigma_{\text{eqv(HMH),max}} = \sqrt{3}\tau_{\text{max}}$, stress correction factor K_τ can also be written as K_σ.

Two additional deflection correction factors are derived and presented as detailed below.

The first novel Timoshenko & Cowper deflection correction factor can be obtained as follows. Taking into the consideration nominal spring deflection from Eq. (14b) and introducing the additional deflection due to shear correction [19–21,36], maximum spring deflection can now be written as

$$\delta_{\text{Timoshenko}} = \delta_{\text{nom}} + \delta_k = \frac{8F_0 D^3 n}{G d^4} + \frac{F_0 L}{k A G}, \tag{18}$$

where k is the *shear correction factor* [19–21,36], L is the total length of the spring and A is spring cross-sectional area. By neglecting the pitch angle α, length L and cross-sectional area A are given by the following equations:

$$L(\alpha \approx 0) = nD\pi, \quad A = \frac{d^2\pi}{4}. \tag{19a,b}$$

Improved shear correction factor k is adopted from Cowper [36] and can be expressed as

$$k = k_{\text{Cowper}} = \frac{6(1+\nu)}{7+6\nu}, \tag{20}$$

where it can be seen that shear correction k is solely Poisson's factor ν dependent, i.e. $k = k(\nu)$. Finally, after inserting Eqs. (20) and (19a,b) into Eq. (18) and dividing it with nominal deflection δ_{nom} from Eq. (14b), Timoshenko & Cowper (T/C) deflection correction, after considering $C = D/d$ and simplifying, is

$$K_{\delta,\text{T/C}} = \frac{\delta_{\text{Timoshenko}}}{\delta_{\text{nom}}} = 1 + \frac{7+6\nu}{12C^2(1+\nu)}, \tag{21}$$

where, as already noted, pitch angle α is for simplicity neglected in derivation.

The second explicit dimensionless deflection correction factor can also be derived by using Castigliano's energy theorem, as noted by Timoshenko [20]. Timoshenko's (Castigliano's) deflection expression is

$$\delta_{\text{Castigliano/Timoshenko}} = F_0 R^2 L \left[\frac{\sin^2(\alpha)}{EI} + \frac{\cos^2(\alpha)}{GI_p}\beta \right], \tag{22}$$

where $R = D/2$ is the mean spring radius, and I and I_p are spring axial and polar inertia moments, respectively,

$$I = \frac{d^4\pi}{64}, \quad I_p = 2I = \frac{d^4\pi}{32}. \tag{23a,b}$$

Interestingly, β from Eq. (22) is an additional deflection correction factor/parameter, for which Timoshenko cites Göhner. In case C is sufficiently small, factor β should be included and can be written as

$$\beta = 1 + 3\left(\frac{1}{C}\right)^2 \left\{ 16\left[1 - \left(\frac{1}{C}\right)^2\right]\right\}^{-1}, \tag{24}$$

where Timoshenko states that "torsional rigidity GI_p must be multiplied by the correction factor" [20] from Eq. (24). As initial pitch angle α is now fully taken into account in Eq. (22), total spring length L, with regard to Eq. (19a), can be calculated according to a more punctual and consistent general helix length expression

$$L(\alpha \neq 0) = \frac{nD\pi}{\cos(\alpha)}. \tag{25}$$

By using Eqs. (25), (24) and (23a,b), inserting them in Eq. (22), and dividing Eq. (22) with nominal deflection δ_{nom} from Eq. (14b), some mathematical simplifying results with Castigliano/Timoshenko (C/T) are as follows:

$$K_{\delta,\text{C/T}} = \frac{\delta_{\text{Castigliano/Timoshenko}}}{\delta_{\text{nom}}} = \frac{(16C^2 - 13)(1+\nu)\cos(\alpha) + 16(C^2 - 1)\sin(\alpha)\tan(\alpha)}{16(C^2 - 1)(1+\nu)}. \tag{26}$$

By inserting $\beta = 1$ in Eq. (22), Eq. (26) morphs into purely Castigliano governed expression

$$K_{\delta,\text{Cstg}} = \frac{(1+\nu)\cos(\alpha) + \sin(\alpha)\tan(\alpha)}{1+\nu}, \tag{27}$$

where spring index C influence is not taken into account; however, pitch angle α is considered. It can be shown that derived deflection correction from Eq. (26) and Göhner expression for deflection correction factor from Table 1 give almost identical results, as further shown in Fig. 3a, i.e. $K_{\delta,\text{C/T}} \approx K_{\delta,\text{Göhn}}$. It should be noted that as the pitch l is geometrically independent value of diameter d, pitch is for plotting purposes tied to wire diameter d through relation $l = 2 \cdot d$, as shown in Fig. 3 rectangular frame. Introduced expression $\alpha = \arctan[l/(\pi D)]$ is employed for calculating pitch angle α for arbitrary spring index C value. Values of $C = 2 - 25$ are considered for plotting. Conventional steel Poisson's ratio $\nu = 0.3$ is adopted for plotting correction factors. Wahl stress correction factor is for the purpose of plotting appropriately hard-coded with $k_{\text{W}} = 0.615$ value, according to Eq. (17b). All expressions from Table 1 are shown in Fig. 3, including newly derived Eqs. (21) and (26) in Fig. 3a.
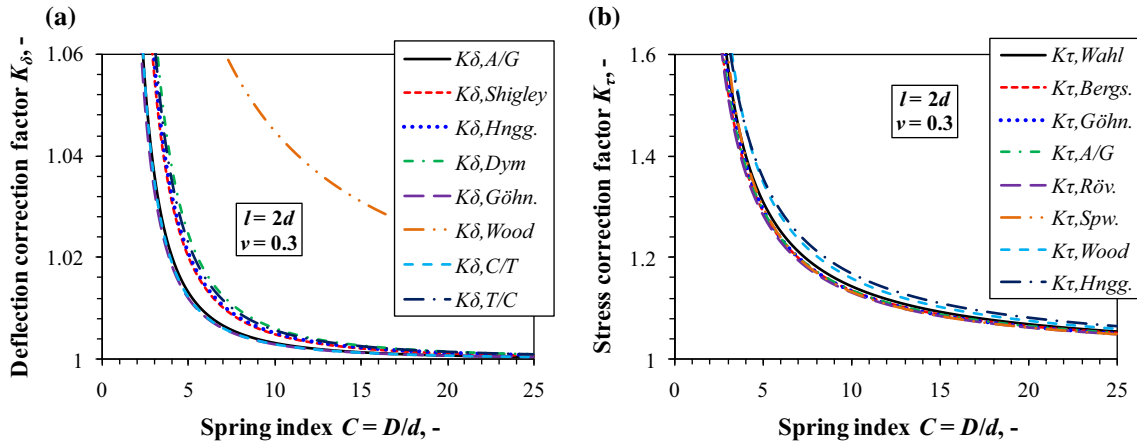
Fig. 3 Different correction factors for $v = 0.3$: **a** deflection correction K_δ, **b** stress correction K_τ (colour figure online)

It can be seen that all plot lines for both deflection and stress factors in Fig. 3 show good mutual correlation, except simple Wood deflection correction expression, which is thus disregarded and excluded from further analyses. It can also be noted that deflection correction factors K_δ contribution are almost one order of magnitude lower compared to stress correction factors K_τ. Neglecting Wood correction expression, Dym [13] presents the largest deflection correction factor. Derived Timoshenko & Cowper deflection correction factor $K_{\delta,\mathrm{T/C}}$ gives higher results compared to other deflection correction curves, however, still lower than Dym. Regarding stress correction, Wood and Honegger give the most conservative results for all values of spring index C.

Assumption that helical spring stress field is purely shear governed and therefore biaxial is employed in fatigue calculation. Adopted von Mises (HMH) $\sqrt{3}K_\tau\tau_{\mathrm{nom}}$ criterion with denoted stress correction factor K_τ is further used. Proportional fatigue stress state is assumed. Proportional stress/strain implies that ratio and/or line direction of principal stresses $\sigma_{1,2,3}$ does not change during fatigue load cycle [4,24], i.e. the orientation of the principal axes with respect to the loading axes remains fixed. For pure shear stress state, relations $\sigma_{1,3} = \pm\tau_{\mathrm{max}}$ and $\sigma_3/\sigma_1 = -1 = \mathrm{const.}$ are valid. By equalling the force amplitudes F_0 from Eq. (14a, b), and by using the defined deflection and stress correction factors, max von Mises equivalent stress amplitude is expressed as

$$\left|\sigma_{\mathrm{eqv(HMH),\ max}}\left(\delta_{\mathrm{max}}\right)\right| \equiv S_{\mathrm{a}} = \sqrt{3}\frac{K_\tau}{K_\delta}\frac{G}{C^2 n \pi d}\delta_{\mathrm{max}}, \tag{28}$$

where S_{a} denotes max fatigue stress amplitude as a function of max deflection amplitude δ_{max}. In order to tie fatigue nomenclature to vibrations, δ_{max} can be obtained from Eq. (4), i.e. relation $\delta_{\mathrm{max}} \equiv |x_{02}|$ holds. Classic HCF Basquin relation [24] for explicit number of cycles N_{f} can be written as

$$N_{\mathrm{f}} = \left(\frac{S_{\mathrm{a}}}{S_{\mathrm{f}}'}\right)^{\frac{1}{B}}, \tag{29}$$

By inserting Eq. (28) in Eq. (29) and using appropriate vibration terminology, i.e. obtained displacement amplitudes from Eq. (4), number of cycles to failure N_{f} can finally be explicitly written as

$$N_{\mathrm{f}} = \left[\sqrt{3}\frac{K_\tau}{K_\delta}\frac{G}{C^2 n \pi d}\frac{|x_{02}\left(\varOmega\right)|}{S_{\mathrm{f}}'}\right]^{\frac{1}{B}}, \tag{30}$$

Advantage of employing simple Eq. (30) is that it is not necessary to explicitly know force amplitude F_0 acting on spring k_3, i.e. mass m_2; however, vibration displacement/deflection amplitudes should be determined before fatigue calculation. Also, it is necessary to know true deflection correction factor K_δ and stress correction factor K_τ, together with relevant fatigue parameters, i.e. fatigue strength coefficient S_{f}' and Basquin's exponent B. In addition, Shigley [22] recommends using factor k_c (*load modification factor*) and multiplying it with S_{f}' in Eq. (29), where $k_c = 0.59$ for torsion. Fatemi et al. [24] mention k_{L} (*empirical load factor*) where $k_{\mathrm{L}} = 0.58$ for torsion, while Bannantine et al. [26] introduce *loading effect* k_{T} which is the most conservative, and for

Table 2 Example 2-DOF vibration isolation system parameters

m_1, kg	m_2, kg	k_1, N/mm	k_2, N/mm	k_3, N/mm	F_0, kN
m_0	$2 \cdot m_0$	k_0	$k_0/10$	k_0	1

Table 3 Example helical spring of stiffness k_0 geometric and material properties

D, mm	d, mm	n, –	l, mm	E, MPa	ν, –	S'_f, MPa	B, –
50	17	1	$2 \cdot d$	200,000	0.3	925	−0.1
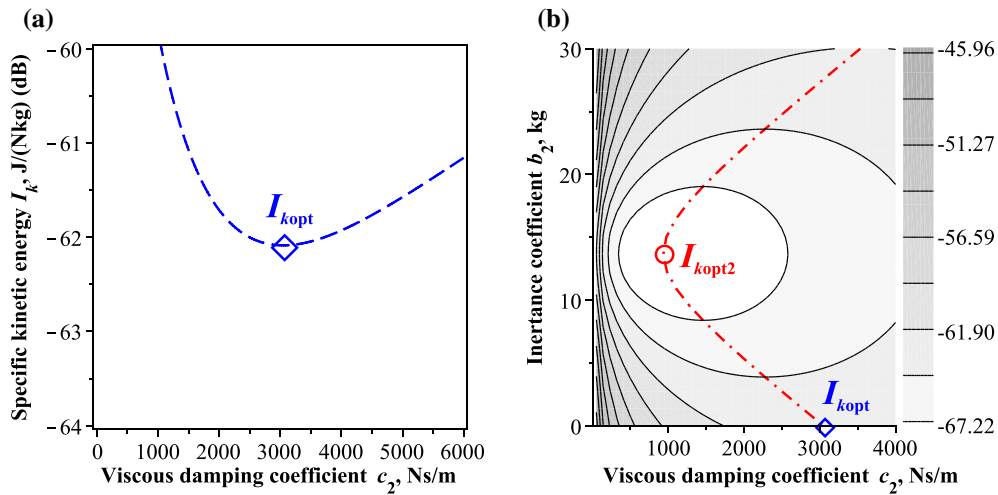
Fig. 4 Mass m_2 specific kinetic energy index I_k: **a** $c_2 = c_{opt}$ and $b_2 = 0$, **b** $c_2 = c_{opt2}$ and $b_2 = b_{opt}$ (colour figure online)

torsion $k_T = 0.577$. Bannantine explains all given values with energy effect theory, i.e. herein previously adopted *von Mises failure criterion* where $1/\sqrt{3} \approx 0.5774$.

In the next chapter, benchmark example is demonstrated for chosen deflection correction factor K_δ and stress correction factor K_τ. Based on information from the literature and this chapter, and by visually inspecting Fig. 3a, b for approximate median values, further adopted are *approximate* Ancker & Goodier deflection correction factor where $K_\delta = K_{\delta,A/G}$, and *approximate* Wahl stress correction factor where $K_\tau = K_{\tau,Wahl}$.

4 Example: inerter-based isolator helical spring vibration fatigue study

In this chapter, vibration fatigue analysis and optimization is performed on a general 2-DOF system, as shown in Fig. 1a. Table 2 shows example parameters used in this isolator optimization process. System is detuned, i.e. $m_2 k_1 \neq m_1 k_3$, and spring k_2 is notably compliant, compared to springs $k_{1,3}$.

General mass value is chosen as $m_0 = 100$ kg and spring stiffness k_0 is yet to be determined from helical spring parameters given in Table 3. Spring material parameters (E, ν, S'_f and B) are chosen in such way to represent physical elastic and fatigue properties of regular spring steel [24,25].

Diameters D and d are chosen so $C = D/d = 50/17 \approx 2.941$ which is a very small spring index. However, such small spring index C results with a relatively large stress correction factor which is a convenient fatigue benchmark. Ideal *massless* springs are considered for simplicity and straightforwardness. Spring stiffness is calculated according to relation $K_\delta F_0 = k_0 \delta_{nom}$. Figure 4 shows plotted numerical results of optimization process for given parameters from Tables 2 and 3. Minimum, i.e. optimum kinetic energy I_{kopt} is determined for the cases without inerter (Fig. 4a—c_{opt}) which corresponds to I_{kopt}, and with inerter (Fig. 4b—c_{opt2} and b_{opt}) which corresponds to I_{kopt2}, by using the method described in Sects. 2.1 and 2.2. Diamond shape in the bottom of Fig. 4b corresponds to the case when $b_2 = 0$, i.e. Fig. 4a. Dash-dotted line in Fig. 4b which connects I_{kopt} and I_{kopt2} represents the implicit plot of function $c_{2(opt)}(b_2 \neq 0)$, i.e. Eq. (13).

Obtained 2-DOF key values/factors and optimized parameters are further listed in Table 4.

Table 4 Example 2-DOF vibration isolation system referent values and optimized parameters

$C = D/d, -$	$K_{\delta, \text{A/G}}, -$	$K_{\tau, \text{Wahl}}, -$	k_0, N/mm	c_{opt}, Ns/m	b_{opt}, kg	c_{opt2}, Ns/m
2.941176471	1.037789623	1.595594406	6 190.746	3 047.31349	13.700475	934.329293
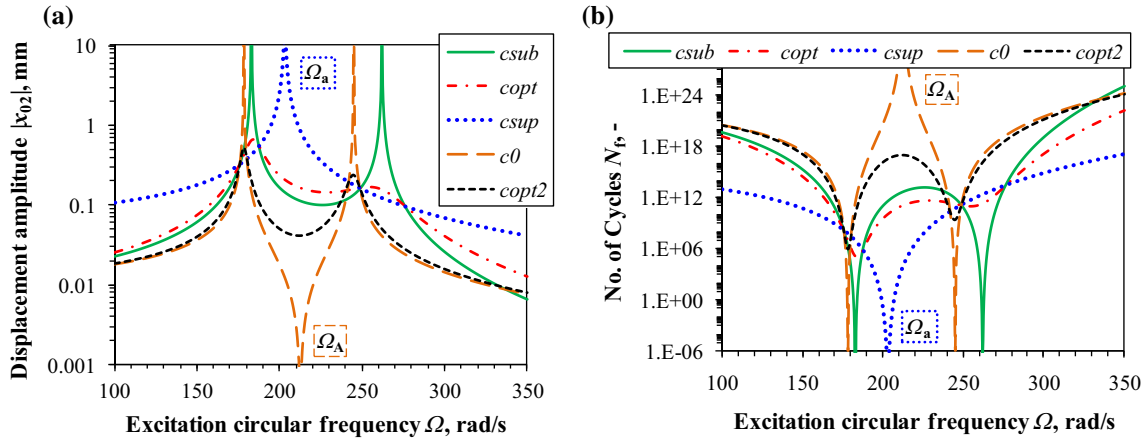
Fig. 5 The 2-DOF frequency response functions: **a** mass m_2 displacement amplitude $|x_{02}|$, **b** spring k_3 number of cycles to fatigue failure N_{f} (colour figure online)

Analytically obtained optimized parameters are used in the fatigue analysis of the spring k_3 which is considered next. Type of spring processing and manufacture, e.g. shot-peening described by SAE [15], Shigley [22], Ugural [23] and Fatemi [24], is not considered. Spring is for simplicity considered to be perfectly smooth and without any residual stresses. Also, spring fatigue notch sensitivity is presumed to be near unity, i.e. $K_{\text{t}(\tau)} \approx K_{\text{f}}$ which is a valid assumption according to Ugural [23]. Spring fatigue life N_{f} can now be calculated according to beforehand derived Eq. (30) where both displacement (A/G) and stress (Wahl) correction factors are taken into account. Analytical FRFs and vibration fatigue results for various cases are shown in Fig. 5.

By comparing FRFs, i.e. displacement amplitudes from Fig. 5a and number of cycles to fatigue from Fig. 5b, similitude of responses can be observed which arises from the fact that spring displacement is linearly proportional to stress, which is nonlinearly, i.e. exponentially proportional to number of cycles to failure, as shown in Eq. (30). Thus, observations for Fig. 5a are also valid for Fig. 5b. Sub-optimal and super-optimal damping are also considered for comparison where $c_{\text{sub}} = c_{\text{opt}}/100$ and $c_{\text{sup}} = 100 \cdot c_{\text{opt}}$. For additional reference, case with optimum inertance $b_2 = b_{\text{opt}}$ is also plotted for zero damping, i.e. $c_2 = c_0 = 0$. The improvement in the number of cycles to failure N_{f} is evident at most frequencies when using the optimum damping c_{opt} in comparison with low damping $c_{\text{sub}} = c_{\text{opt}}/100$, or high damping $c_{\text{sup}} = 100 \cdot c_{\text{opt}}$. Additionally, a significant further improvement in the fatigue life N_{f} is observed at most frequencies, in case where the optimum inerter b_{opt} is implemented in combination with the optimum damper c_{opt2}. Interesting anti-resonance phenomenon at frequency Ω_{A} is observed for the case with the optimum inerter b_{opt} and without damping ($c_2 = c_0 = 0$), which specifically demonstrates inerter b_2 influence that otherwise cannot be achieved on the receiving body by using only classic elements of MDS system [38]. Contrary to that, if using very large damping in the isolator, i.e. $c_{\text{sup}} = 100 \cdot c_{\text{opt}}$, new resonance Ω_{a} can be observed, as two masses m_1 and m_2 vibrate together in phase with equal displacements, velocities, and accelerations, acting as a quasi-rigid body. Same effect can be observed if a very large spring stiffness k_2 is used in the isolator, as isolator effectively locks and its proper functionality is consequently permanently compromised. Similar conclusion is already drawn based on $I_{k\text{opt}}$ structure of Eq. (12).

In summary, six characteristic circular frequencies denoted further in Fig. 6 are observed. These are: two circular natural frequencies for the case without inerter ($b_2 = 0$), i.e. ω_{n1b0} and ω_{n2b0} in Fig. 6a, two circular natural frequencies for the case with inerter ($b_2 = b_{\text{opt}}$), i.e. $\omega_{n1b\text{opt}}$ and $\omega_{n2b\text{opt}}$ in Fig. 6b, anti-resonant circular frequency $\Omega_{\text{A}}(b_2 = b_{\text{opt}})$ in Fig. 6b and isolator-locking resonant circular frequency $\Omega_{\text{a}}(c_2, k_2 \to \infty)$ in Fig. 6a. Circular natural frequencies can be obtained by solving the eigenvalue problem for the given 2-DOF as

$$\left[\mathbf{K} - \left(\omega_{n1,2} \right)^2 \mathbf{M} \right] \mathbf{x}(t) = 0 \tag{31}$$
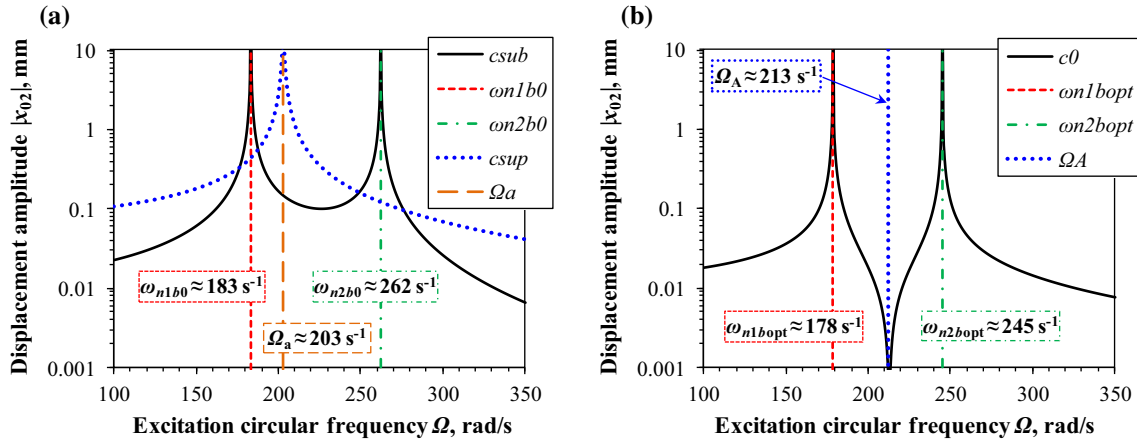
Fig. 6 Characteristic circular frequencies and accompanying FRFs: **a** $c_2 = c_{\text{sub}}$ and $c_2 = c_{\text{sup}}$, $b_2 = 0$, **b** $c_2 = 0$, $b_2 = b_{\text{opt}}$ (colour figure online)

Table 5 Characteristic circular frequencies: **a** without inerter ($b_2 = 0$), **b** with optimum inertance ($b_2 = b_{\text{opt}}$)

	ω_{n1b0}, rad/s	ω_{n2b0}, rad/s	Ω_{a}, rad/s		$\omega_{n1b\text{opt}}$, rad/s	$\omega_{n2b\text{opt}}$, rad/s	Ω_{A}, rad/s
(a)	183.017	262.015	203.154	**(b)**	178.373	244.852	212.571

Table 6 The 2-DOF isolator vibration fatigue optimization results

Isolator type	Ω, rad/s	$|x_{02}(\Omega)|$, mm	$N_{\text{f}}(\Omega)$, –
Sub-optimal damping ($c_2 = c_{\text{opt}}/100$, $b_2 = 0$)	ω_{n1b0}	47.583	$<< 1$
Super-optimal damping ($c_2 = 100 \cdot c_{\text{opt}}$, $b_2 = 0$)	Ω_{a}	14.539	< 1
Optimal damping ($c_2 = c_{\text{opt}}$, $b_2 = 0$)	ω_{n1b0}	0.640	134,539
Optimal damping and inertance ($c_2 = c_{\text{opt2}}$, $b_2 = b_{\text{opt}}$)	$\omega_{n1b\text{opt}}$	0.524	1,002,948

where **M** and **K** matrices are denoted in Eq. (2a,c). Inserting data from Table 2 into Eq. (31) yields with

$$\left(\omega_{n1,2}\right)^2 = \frac{\frac{33}{10}m_0 k_0 + 2b_2 k_0 \mp \sqrt{\frac{129}{100}m_0^2 k_0^2 - \frac{6}{5}b_2 m_0 k_0^2 + 4k_0^2 b_2^2}}{2\left(2m_0^2 + 3m_0 b_2\right)}, \tag{32}$$

where inertance b_2 can be arbitrarily defined, or set to zero nevertheless. Following expressions

$$\Omega_{\text{A}} = \sqrt{\frac{k_2}{b_2}}, \quad \lim_{c_2, k_2 \to \infty} \Omega_{\text{a}} = \sqrt{\frac{k_1 + k_3}{m_1 + m_2}}, \tag{33a,b}$$

denote anti-resonance Ω_{A} and locking resonant circular frequency Ω_{a}, respectively. Table 5 shows Eqs. (32) and (33a,b) algebraic solutions by inserting data from Table 4 for the cases without, and with inerter where $b_2 = b_{\text{opt}}$.

Figure 6 presents characteristic frequencies data from Table 5 combined with belonging FRFs.

For small damping values, i.e. $c_2 \approx 0$, system response in wide frequency range is governed purely by natural frequencies vicinity where very large vibration amplitudes occur. For very large values of either damping c_2 and/or spring stiffness k_2, isolator effectively locks even with the inerter present, i.e. for c_2, $k_2 \to \infty$, $\Omega_{\text{a}}(b_2 = 0) = \Omega_{\text{a}}(b_2 = b_{\text{opt}})$. This is unfavourable setup and should be avoided, because if excited, locking frequency Ω_{a} vibration amplitudes tend to infinity, as demonstrated in Figs. 5a, b and 6a (c_{sup} curves, dotted line). In order to evaluate the quality of performed vibration isolation optimization, Table 6 is presented. Four characteristic system results are denoted where the most destructive excitation frequency Ω is solely considered.

For systems with sub- and super-optimal damping, violent spring rupture occurs for given loading immediately, without even considering fatigue failure. Optimized damping c_{opt} shifts the life of observed spring in

HCF range with over 10^5 expected life cycles. Finally, simultaneous optimization of damping and inertance shifts the expected life cycles over the 10^6 range, which can be considered as a significant improvement.

The present optimization is based on a vibration-related specific kinetic energy criterion. A future work could consider a type of optimization which would aim at directly maximizing fatigue life of the spring and compare it to the present results. Considering that pitch angle in the present study is defined through relation $l = 2 \cdot d$ and $\alpha = \arctan[l/(\pi D)]$, it would be beneficiary to further investigate the influence of arbitrary large pitch angle α on deflection and stress correction, as some of the expressions from Table 1 consider the pitch angle influence, and some do not. That most notably applies to further evaluation of Wahl's approximate stress correction factor in detail. Continuation of this work could also be the investigation of mean stress σ_m influence on the spring fatigue life optimization, as present calculations were performed for a simple harmonic fully reversed loading $R = -1$ where dead weight static load, or general pre-stress were not considered. In addition to a demonstrated analytical study, numerical method for verification purposes will be further employed as a continuation of this paper. Software packages which use FEM generated static/dynamic multi-axial complex stress fields for predicting fatigue life will be used.

5 Conclusion

A cylindrical spring fatigue optimization method for inerter-based vibration isolation system is presented in this paper. The method is demonstrated on a simple discrete two-degree-of-freedom system. A simplified model for calculating cylindrical spring high-cycle fatigue life is established by adopting von Mises energy criterion for shear governed biaxial proportional stress and relating it to spring displacement amplitudes in Basquin's equation. Most convenient deflection and stress correction factors are adopted for vibration fatigue study, namely Ancker & Goodier deflection correction and Wahl stress correction factor. Two additional displacement correction factors are derived and compared to other referent solutions.

Two main benchmark isolators are investigated; one with inerter of optimal inertance and optimal damping, and one with optimal damping but without the inerter. These two plain isolator systems are viewed as a simplified model of a possibly more complicated dynamic structure. Parameters of the inerter-based isolator are optimized to maximize the effect of vibration isolation, which also corresponds to significant reductions of the stresses in the considered receiving body spring and an increase of its fatigue life as a consequence. It is demonstrated that the vibration isolation effect of the isolator not containing the inerter can be substantially improved by employing the ideal inerter in parallel with the isolator spring and viscous damper. Hence, it can be concluded that minimizing the kinetic energy of the receiving body, by employing inerter of adequate, i.e. optimized inertance, can convincingly prolong the coupling helical spring fatigue life. Specifically inerter anti-resonance effects can also be potentially used to fine tune the system for one dominant excitation frequency, and significantly reduce vibration amplitudes on that particular frequency.

As a direct continuation of this work, finite element method will be employed for results verification purposes. Main challenges are to implement ideal inerter concept in the finite element model and to well correlate spring displacements and stresses obtained by the developed analytical model to the results obtained by the finite element analysis.

References

1. Rao, S.S.: Mechanical Vibrations, 5th edn. Prentice Hall, New York (2010)
2. Smith, M.C.: Synthesis of mechanical networks: the inerter. IEEE Trans. Autom. Control **47**(10), 1648–1662 (2002)
3. Steinberg, D.S.: Vibration Analysis for Electronic Equipment, Third edn. Wiley, New York (2000)
4. Bishop, N.W.M., Sherratt, F.: Finite Element Based Fatigue Calculations. NAFEMS, Farnham (2000)
5. Lee, Y., Barkey, M.E., Kang, H.: Metal Fatigue Analysis Handbook. Practical Problem-Solving Techniques for Computer-Aided Engineering. Elsevier, Waltham (2012)
6. Wahl, A.M.: Helical compression and tension springs. ASME paper A-38. J. Appl. Mech. **2**(1), A-35–A-37 (1935)
7. Wahl, A.M.: Mechanical Springs, 1st edn. Penton, Cleveland (1944)
8. DIN EN 2089-1-1963-01 (1963) Helical Springs Made From Round Wire and Rod—Calculation and Design of Compression Springs
9. DIN EN 2089-1-1963-02 (1963) Helical Springs Made From Round Wire and Rod—Calculation and Design of Tension Springs

10. Din EN 13906-1: Cylindrical Helical Springs Made From Round Wire and Bar—Calculation and Design—Part 1: Compression Springs. BeuthVerlag, Berlin (2002)
11. Din EN 13906-2: Cylindrical Helical Springs Made From Round Wire and Bar—Calculation and Design—Part 2: Extension Springs. BeuthVerlag, Berlin (2002)
12. Ancker Jr., C.J., Goodier, J.N.: Pitch and curvature correction for helical springs. ASME J. Appl. Mech. **25**(4), 466–470 (1958)
13. Dym, C.L.: Consistent derivations of spring rates for helical springs. ASME J. Mech. Des. **131**(7), 1–5 (2009)
14. Research Committee on the Analysis of Helical Spring: Report of research committee on the analysis of helical spring. Trans. Jpn. Soc. Spring Eng. **2004**(49), 35–75 (2004)
15. Society of Automotive Engineers (SAE): Spring Design Manual. Ae Series. Society of Automotive Engineers Inc., Warrendale (1990)
16. Hearn, E.J.: Mechanics of Materials, Volume 1, An Introduction to the Mechanics of Elastic and Plastic Deformation of Solids and Structural Materials, 3rd edn. Butterworth-Heinemann, Oxford (1997)
17. Meissner, M., Schorcht, H.-J., Kletzin, U.: Metallfedern: Grundlagen, Werkstoffe, Berechnung, Gestaltung und Rechnereinsatz, 3rd edn. Springer, Berlin (2015)
18. Shimoseki, M., Hamano, T., Imaizumi, T.: FEM for Springs. Springer, Berlin (2003)
19. Timoshenko, S.P.: Strength of Materials, Part I, Elementary Theory and Problems, 2nd edn. D. Van Nostrand, New York (1940)
20. Timoshenko, S.P.: Strength of Materials, Part II, Advanced Theory and Problems, 2nd edn. D. Van Nostrand, New York (1940)
21. Timoshenko, S.P., Goodier, J.N.: Theory of Elasticity, 2nd edn. McGraw-Hill, New York (1951)
22. Budynas, R.G., Nisbett, J.K.: Shigley's Mechanical Engineering Design, 10th edn. McGraw-Hill, New York (2015)
23. Ugural, A.C.: Mechanical Design of Machine Components, 2nd edn. CRC Press, Boca Raton (2015)
24. Stephens, R.I., Fatemi, A., Stephens, R.R., Fuchs, H.O.: Metal Fatigue in Engineering, 2nd edn. Wiley, New York (2005)
25. Roessle, M.L., Fatemi, A.: Strain-controlled fatigue properties of steels and some simple approximations. Int. J. Fatigue **22**(6), 495–511 (2000)
26. Bannantine, J.A., Comer, J.J., Handrock, J.L.: Fundamentals of Metal Fatigue Analysis. Prentice Hall, Englewood Cliffs (1990)
27. Romanowicz, P.: Numerical assessment of fatigue load capacity of cylindrical crane wheel using multiaxial high-cycle fatigue criteria. Arch. Appl. Mech. **87**, 1707–1726 (2017)
28. Berger, C., Kaiser, B.: Result of very high cycle fatigue tests on helical compression springs. Int. J. Fatigue **28**, 1658–1663 (2006)
29. Kaiser, B., Berger, C.: Fatigue behaviour of technical springs. Mater. Werkst. **36**(11), 685–696 (2005)
30. Del Llano-Vizcaya, L., Rubio-González, C., Mesmacque, G., Cervantes-Hernandez, T.: Multiaxial fatigue and failure analysis of helical compression springs. Eng. Fail. Anal. **13**(8), 1303–1313 (2006)
31. Pyttel, B., Ray, K.K., Brunner, I., Tiwari, A., Kaoua, S.A.: Investigation of probable failure position in helical compression springs used in fuel injection system of diesel engines. IOSR J. Mech. Civil Eng. **2**(3), 24–29 (2012)
32. Rivera, R., Chiminelli, A., Gómez, C., Núñez, J.L.: Fatigue failure analysis of a spring for elevator doors. Eng. Fail. Anal. **17**(4), 731–738 (2010)
33. Ružička, M., Doubrava, K.: Loading regimes and designing helical coiled springs for safe fatigue life. Res. Agr. Eng. **51**(2), 50–55 (2005)
34. Kamal, M., Rahman, M.M.: Finite element-based fatigue behaviour of springs in automobile suspension. Int. J. Autom. Mech. Eng. **10**, 1910–1919 (2014)
35. Kuznetsov, A., Mammadov, M., Sultan, I., Hajilarov, E.: Optimization of improved suspension system with inerter device of the quarter-car model in vibration analysis. Arch. Appl. Mech. **81**, 1427–1437 (2011)
36. Cowper, G.R.: The shear coefficients in Timoshenko's beam theory. ASME J. Appl. Mech. **33**(2), 335–340 (1966)
37. Mlikota, M., Schmauder, S., Božić, Ž., Hummel, M.: Modelling of overload effects on fatigue crack initiation in case of carbon steel. Fatigue Fract. Eng. Mater. Struct., Special Issue: 16th International Conference on New Trends in Fatigue and Fracture (NT2F16) 40(8):1182–1190 (2017)
38. Alujević, N., Čakmak, D., Wolf, H., Jokić, M.: Passive and active vibration isolation systems using inerter. J. Sound Vib. **418**, 163–183 (2018)
39. Alujević, N., Wolf, H., Gardonio, P., Tomac, I.: Stability and performance limits for active vibration isolation using blended velocity feedback. J. Sound Vib. **330**, 4981–4997 (2011)
40. Alujević, N., Gardonio, P., Frampton, K.D.: Smart double panel for the sound radiation control: blended velocity feedback. AIAA J. **49**(6), 1123–1134 (2011)
41. Caiazzo, A., Alujević, N., Pluymers, B., Desmet, W.: Active control of turbulent boundary layer-induced sound transmission through the cavity-backed double panels. J. Sound Vib. **422**, 161–188 (2018)
42. James, H.M., Nichols, N.B., Phillips, R.S.: Theory of Servomechanisms. MIT Radiation Laboratory Series, vol. 25, First edn. McGraw-Hill, New York (1947)

Publisher's Note Springer Nature remains neutral with regard to jurisdictional claims in published maps and institutional affiliations.